Research Article | Vol. 10, No. 4 | 1 Apr 2019 | BIOMEDICAL OPTICS EXPRESS 1750
Biomedical Optics EXPRESS

Nonlinear Brillouin spectroscopy: what makes it a better tool for biological viscoelastic measurements

CHARLES W. BALLMANN,[1] ZHAOKAI MENG,[1] AND VLADISLAV V. YAKOVLEV[1,2,*]

[1]*Texas A&M University, College Station, TX 77843-4242, USA*
[2]*Zhejiang University, Hangzhou, Zhejiang 310027, China*
[*]*yakovlev@tamu.edu*

Abstract: Brillouin spectroscopy is an emerging tool in biomedical imaging and sensing. It is capable of assessing the high-frequency viscoelastic longitudinal modulus with microscopic spatial resolution. Nonlinear Brillouin spectroscopy based on impulsive stimulated Brillouin scattering offers a number of significant advantages over conventional spontaneous and stimulated Brillouin scattering. In this report, we evaluate the accuracy of Brillouin shift measurements in spontaneous and nonlinear Brillouin microscopy by calculating the Allan variance for both CW excited spontaneous Brillouin measurements and nonlinear Brillouin scattering measurements made with both nanosecond and picosecond pulse excitation. We find that impulsive stimulated Brillouin spectroscopy is superior to spontaneous Brillouin spectroscopy in terms of the accuracy of such measurements and demonstrate its application for assessing tiny changes in Brillouin frequency shifts associated with low concentrations of biologically relevant solutions.

1. Introduction

Elastic properties of molecular, sub-cellular and cellular structures play a crucial role in many areas of Biology and Medicine. A prominent example is cancer diagnostics and imaging, where abnormal elastic properties of cancer cells and their local extracellular matrix (ECM) serve as unique markers for cancer [1]. Many disease processes involve pathological changes in tissue stiffness [2–4], providing an early diagnostic tool for disease development. More broadly, fundamental understanding of embryonic development [5], mechanotransduction [6], infection diseases [7], and advanced biomaterials with superior mechanical properties [8] calls for the development new tools and methodologies for assessment of elastic properties of tissues [9]. Brillouin spectroscopy, which is an inelastic scattering of light by sound waves in a medium by thermal or electrostrictive excitation [10], is capable of providing such information [11, 12] through confocal microscopic imaging [13–15]. A growing number of applications reaffirms Brillouin spectroscopy as an emerging tool of biomedical imaging [16–24]. Spontaneous Brillouin microscopy remains a method of choice due to the growing availability of high-resolution spectrometers. Nonlinear Brillouin microscopy was originally introduced in the form of stimulated Brillouin microscopy [25], which was proven to provide a better imaging capability through a scattering medium [26]. However, the overall complexity of the experimental setup required for attaining a high resolution Brillouin spectrum for exact Brillouin shift and linewidth assessment prompted the use of impulsive stimulated Brillouin scattering (ISBS) [27, 28] to overcome these shortcomings [29, 30]. ISBS can be implemented by first generating a transient density grating in a material by intersecting two beams of high intensity laser pulses in the material. This grating is then probed by a weaker pulsed or CW laser by Bragg scattering off of the grating. Since this grating is moving, it will modulate the probe beam which is detected with a photodiode. Data collection for ISBS is very fast compared with the above imaging

#354440 https://doi.org/10.1364/BOE.10.001750
Journal © 2019 Received 3 Dec 2018; revised 1 Feb 2019; accepted 1 Feb 2019; published 8 Mar 2019

Biomedical Optics EXPRESS

methods. Also, unlike counterpropagating stimulated Brillouin scattering, ISBS allows one to use broad bandwidth, high intensity lasers for the pump without affecting the frequency resolution. In this case the frequency resolution depends on things such as phonon lifetime, beam geometry at the focus and collection time length. Since broadband lasers can be used, one can take advantage of the high intensities from these type laser sources to obtain orders of magnitude higher signal than in the CW case. As a result, the signal is collected much fast than in conventional Brillouin spectroscopy. However, fast acquisitions do not always result in an improved signal-to-noise ratio, as was demonstrated earlier for nonlinear Raman spectroscopy (see, for example, [31]). Brillouin spectroscopy of biological systems often relies on minute variations of the Brillouin shift and linewidth, and careful analysis of the Brillouin signal is needed for extracting information about local viscoelastic properties [19, 32]. More recently, the performance of modern Brillouin spectroscopy systems was evaluated and compared in terms of their accuracy in measuring the Brillouin shift [33]. While spontaneous Brillouin spectroscopy and ISBS are important techniques and have a proper place in material characterization and biological spectroscopy and microscopy, there is a need to provide accurate measurements with the highest possible precision over an extended period of time. Thus, it would be of great interest to have a performance rubric in order to compare between the two techniques and determine which method is most appropriate for the task at hand. This is especially important to establish optimal power and/or pulse intensity (or pulse length) parameters for imaging cells and tissues that are moving or are easily damaged. It is the goal of this work to provide such a comparison. The manuscript is arranged as follows. After a short theoretical introduction, we provide a brief overview of the experimental configurations used and present the data, collected for different experimental arrangements, paying special attention to the data statistics in order to determine optimal samples needed for minimum uncertainty. We then compare both spontaneous Brillouin and ISBS spectroscopies in the discussion section and show how ISBS can be used to evaluate viscoelastic properties of solutions with a small variation of chemical composition.

2. Theory

Spontaneous Brillouin scattering arises from the scattering of light from thermodynamic adiabatic density fluctuations (acoustic fluctuations) inherent in any material. The first published theoretic framework on light scattering from acoustic fluctuations was by L. Brillouin in 1922 [34]. A beam of light enters a medium and scatters off of the acoustic fluctuations in the medium. The scattered light is shifted in frequency by $\pm\Omega$ where Ω is the frequency of the acoustic wave. This shift can be expressed in the following equation,

$$\Omega = 2|\mathbf{k}|\upsilon \sin(\Theta/2) = 2n\omega\beta \sin(\Theta/2) \tag{1}$$

where $\mathbf{k}$ and ω are the wavevector and frequency of the incident light, n is the index of refraction, $\beta = \frac{\upsilon}{c}$ where υ is the speed of sound in the material and c is the vacuum speed of light, and Θ is the angle between incident and scattered light.

The scattering off of spontaneous acoustic waves yields a weak signal, and this signal can be dwarfed by spontaneous Rayleigh scattering if special filtering is not implemented. Stimulated Brillouin scattering can provide a much larger signal and is not plagued by the spontaneous Rayleigh background. ISBS, a form of SBS, has many advantages over traditional SBS such as the ability to control the frequency of the phonon created, the ability to use a pulsed pump source with a narrow-band probe, and ease of implementation.

In ISBS, the pump beam is split in two and then intersected again inside the sample. The interference pattern at the intersection of the two pump beams will form a transient density

Biomedical Optics EXPRESS

grating in the medium. The period of this grating is given by,

$$\Lambda = \frac{\lambda_{\text{pump}}}{2\,\sin(\theta_{\text{pump}}/2)} \tag{2}$$

where λ_{pump} is the pump wavelength and θ_{pump} is the angle of intersection of the two pump beams. The probe beam, which can be a single beam or two beams in a heterodyne configuration, is Bragg scattered off of this transient grating and collected with a photodiode. Bragg scattering of a beam of light off of a transient grating, formed by standing wave interference in a material from another light beam, was first observed experimentally in 1967 by Boersch and Eichler [35]. A detailed compilation of theoretical and experimental work on dynamic gratings can be found in Ref. [36]. In our setup, we use an approach [37] which uses a phase mask image which is refocused on the sample as seen in Fig. 1.

In this way, the Bragg condition is already satisfied so that difficult alignment, as well as delay lines, are avoided. The induced grating wavelength can be expressed as [28],

$$\Lambda = \left(\frac{f_2}{f_1}\right)\frac{\Lambda_0}{2}, \tag{3}$$

where Λ_0 is the grating period and f_1 and f_2 are focal lengths of the two imaging lenses (see Fig. 1). The output frequency can then be expressed as

$$f_{signal} = \frac{\upsilon}{\Lambda}, \tag{4}$$

where υ is the speed of sound in the material. We can then use the diffracted and reference beams in an optical heterodyne detection configuration [28] to increase the signal, which is given by

$$I_S = I_{Ref} + I_R + 2\sqrt{I_{Ref} I_R}\ \cos\left(\theta_p\right), \tag{5}$$

where θ_p is the phase difference between I_{ref} and I_R and $I_R = \eta I_D$ (η is the diffraction efficiency) is the diffracted portion of I_D. The last term in equation 5 is what is of interest since the signal is multiplied by the reference signal. This amplification effect is one of the main reasons for this heterodyne detection scheme.

3. Experimental setup

The simplified experimental setups for ISBS and SpBS are shown in Fig. 1 and Fig. 2. For ISBS (Fig. 1), the pump laser is changed between a nanosecond or picosecond laser. The probe was a diode laser (Newport, Inc.; Vortex II TLB-6900) with 45 mW total power at 780 nm. The pump laser used for nanosecond data was a 532 nm, 1 ns fiber laser (IPG Photonics, Corp.; GLPR-10) with ~ 0.5 μJ pulse energy at the sample at 100 kHz, and for the picosecond data we used a 532 nm, 6 ps hybrid fiber/free space amplified laser (Attodyne, Inc.; APLX-1064-532) with the power attenuated to give ~ 0.5 μJ at the sample at 100 kHz. The pump and probe beams are combined with a cold mirror and focused on the transmission grating (48 μm grating period) in the vertical direction using a cylindrical lens (10 cm focal length). Using a 4f lens system (f_1 and f_2 are 75 and 25.4 mm, respectively), the grating is then re-imaged into the sample. After the sample, everything but the signal is blocked by a slit.

A cold mirror blocks most of the stray 532 nm beam coming through, however a 750 longpass filter in conjunction with a 532 notch filter are used to further remove any remaining pump light. The signal is focused onto a photodiode (Thorlabs; DET10A) which is connected to a 350 MHz preamplifier (Stanford Research Systems; Model SR445A) and then sent to an oscilloscope (Agilent Technologies; DSO6034A, 300 MHz) for data collection. The oscilloscope is triggered

Biomedical Optics EXPRESS

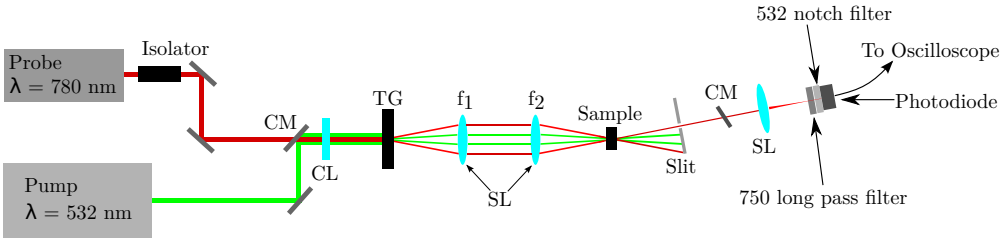

Fig. 1. Simplified schematic of the ISBS setup. The two beams are loosely focused on a transmission grating (TG) and re-imaged on the sample. The signal is then optically filtered and sent to the photodiode. CL - Cylindrical Lens, SL - Spherical Lens, CM - Cold mirror (all other unmarked mirrors are dielectric)

from another photodiode at the pump output. The data is collected on a computer from the oscilloscope using a custom NI LabVIEW™ code.

Figure 2 shows a simplified schematic of our SpBS setup that starts with a diode seed laser (Pure Photonics, LLC; PPCL300) with center wavelength around 1560.48 nm which is input into a fiber amplifier (IPG Photonics, Corp.; EAR-5K-C-LP-SF). The output of the amplifier is passed through a second harmonic crystal (Covesion, Ltd.; MgO:PPLN, MSHG1550-1.0-20) where the output is now at the D_2 resonance in Rb ($\simeq$ 780.24 nm). The beam is reflected by a polarization cube and then passes through a $\lambda/4$ waveplate before it is then focused on the sample. The signal light then passes through the $\lambda/4$ waveplate and now passes through the polarization cube. This allows collection of all the backscattered light verses using a conventional beam splitter. The Rayleigh scattered light is then filtered [38] from the signal beam by double passing it through a warm Rb cell ($\sim 60 - 70$ °C). The signal is then focused into a VIPA and the far field image is collected with a CCD (Andor Technology, Ltd.; Neo 5.5 sCMOS).

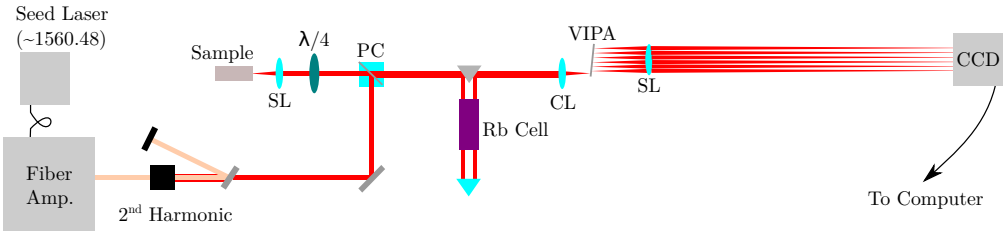

Fig. 2. Simplified schematic of the SpBS setup. After the interaction the spontaneous Rayleigh scattered light is filtered with a Rb cell. The beam is then focused into a VIPA where it is dispersed. The far field image is collected with a CCD and then analyzed. SL - Spherical Lens, CL - Cylindrical Lens, PC - Polarization Cube

4. Results

In the following, we present a statistic comparison of data taken with ISBS and SpBS. For both SpBS and ISBS, many measurements are taken in succession to obtain appropriate statistics of the measurement. Figure 3 shows examples of averaged spectra for SpBS (a) and ISBS (b) of acetone. A typical SpBS spectrum will include three peaks, the Rayleigh peak and the Brillouin Stokes and anti-Stokes peaks. In our case the Rubidium cell filters the Rayleigh peak and leaves the Brillouin peaks. The distance between any two closest peaks (such as between 2 and 4 mm in Fig. 3(a)) is two times the Brillouin shift. Details on how to correct for dispersion from the VIPA to precisely determine the Brillouin shift from all of the peaks can be found in the literature [39].

Biomedical Optics EXPRESS

For ISBS (Fig. 3(b)), the frequency is determined by taking the Fourier transform of the time signal and applying a curve fit to the primary frequency component.

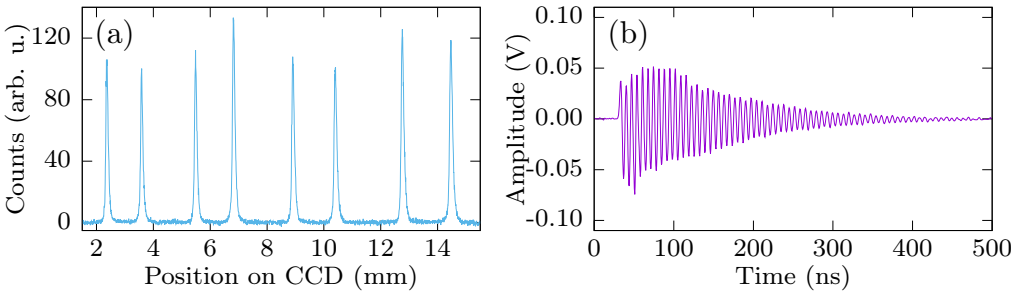

Fig. 3. Averaged sample spectra for SpBS (a) and ISBS (b) of acetone.

Once we have determined the frequencies we perform statistical analysis, namely, the Allan variance of the data. Figure 4 is a plot of the Allan variance [40] for acetone as a function of the measurement time (the number of measurements times the time per measurement). The Allan variance gives a measure of the variance with respect to time, or number of samples (assuming the samples are taken periodically), and shows the influences of both short term and long term noise. The Allan 2-sample variance is given by

$$\sigma_y^2(\tau) = \frac{1}{2}\langle(\bar{y}_{n+1} - \bar{y}_n)^2\rangle, \tag{6}$$

where τ is the observation period and $\bar{y}_i$ is the n'th averaged data block over the observation time τ. In a typical Allan variance plot, the variance starts at some high initial value and drops till it reaches a minimum value, and then will either stay steady or (usually) go back up again. This gives an estimate of how many measurements need to be taken and averaged to achieve a desired uncertainty. Past the minimum, acquiring more samples will only degrade the signal further.

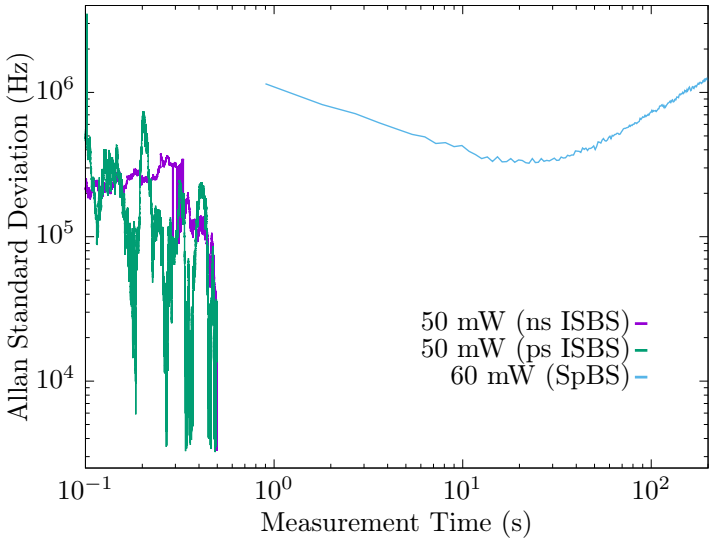

Fig. 4. The Allan standard deviations of the SpBS and ISBS signal of acetone verses measurement time. ISBS achieves a lower uncertainty, and does so orders of magnitude faster. The ISBS signal increases after 0.5 s has been eliminated for clarity of the graph.

Biomedical Optics EXPRESS

In Fig. 4 we see Allan standard deviation plots for SpBS and nanosecond and picosecond ISBS for an acetone sample. For the ISBS curves, the minimum uncertainty is reached at around 50,000 measurements at 50 mW average power. The uncertainty then increases, but has been eliminated for clarity of the graph. The drift of the CW laser for SpBS over 0.5 seconds was measured to be $\leq$1 MHz and is approximately random noise, while the long term drift was on the order of $\approx$ 5 MHz. This long term drift was periodic, which is most likely due to air conditioning cycles of the laboratory. From Fig. 4 we see that this long term drift starts to become appreciable after 25 samples (22.5 s) and is the main reason we do not achieve a lower variance.

It should be noted that in our case, ISBS frequencies were on the order of $\sim$ 100 MHz, while SpBS was $\sim$ GHz. This is the reason that the variance of SpBS is about an order of magnitude higher at the short time intervals compared to ISBS. The coefficient of variation is about the same. There are two very important features from this graph. First, the time it takes ISBS to reach minimum uncertainty is over and order of magnitude less compared to SpBS. Second, even taking the coefficient of variation into account, the minimum uncertainty of ISBS drops many orders of magnitude less than SpBS.

5. Discussion

From the data above, we observe some important differences between SpBS and ISBS. First, we should consider the time it takes to obtain the best data. In our SpBS setup the integration time was set to 0.5 s, however it takes $\simeq$ 0.9 s per data point, since the computer has to process and save the data, and other time delays such as delay from the experiment control code. Therefore, for the best case scenario for SpBS (which is acetone at 60 mW) it takes about 25 samples for minimum uncertainty, which results in $25 \times 0.9 = 22.5$ s. In contrast, ISBS takes around 50,000 samples, with each spectrum taken in 10 μs, which results in $5 \times 10^4 \times 10^{-5} = 0.5$ s total time. This shows quite an improvement over SpBS. The strength of the ISBS signal for the lowest pump power used (50 mW) is $\sim$ 10 nW. For our SpBS setup however, even at 60 mW, the backward signal is at most $\sim$ 100 pW. The flexibility in being able to use pulsed lasers for ISBS results in a much stronger signal, therefore less time is required to reach minimum uncertainty.

Another advantage that ISBS has as compared to SpBS is that one has more flexibility in choosing the proper wavelength for the excitation and detection. As a result, this wavelength can be carefully selected to minimize the stress on cells and tissues [41–43], while the probe wavelength can be matched with the peak of the detection sensitivity of a photodiode. In contrast, SpBS is a spontaneous scattering process and scatters with an intensity proportional to $\frac{1}{\lambda^4}$. Therefore, the wavelength range that will improve your signal the most, namely the UV, is also the most damaging range of frequencies both for materials and physiologically.

Another important comparison is that of frequency stability. In SpBS, the shift is a function of the input frequency. Therefore, laser drift is another source of noise for SpBS. While great care can be taken to thermally isolate the SpBS CW laser from laboratory air currents and employ a phase-locked loop to narrow the linewidth and decrease drift, which will decrease the SpBS uncertainty, this comes with tremendous complexity over the ISBS setup. For ISBS with a phase mask (such as used in this work), the measured frequency is independent of the frequency of the pump or probe.

The spatial resolution of SpBS is governed by the resolution of the optical system, which in microscopy the system typically relies on a large numerical aperture objective. From equation 1 it is evident that the higher the numerical aperture, the larger the observed spontaneous Brillouin linewidth will be. However, the accuracy of the spontaneous Brillouin shift is affected mostly by laser drift and spectrometer resolution. For experiments that are interested in both the spontaneous Brillouin shift and linewidth, great care must be taken to achieve this. For ISBS, the point spread function of the probe beam path sets the spatial resolution (similar to SpBS). In order for efficient diffraction of the probe beam however, the grating period must be on the order of the spot size

Biomedical Optics EXPRESS

of the probe beam or smaller. This will increase the observed ISBS signal frequency. Since oscilloscopes have a finite sample rate for a given time window, then in order to properly sample a waveform, one will have to decrease the observed time window as the observed frequency increases. This will reduce the accuracy of the ISBS modulation frequency measurement. Most ISBS experiments are interested only in the measure frequency, but sometimes the linewidth is desired as well. In general, the ISBS linewidth is determined by many variables such as phonon lifetime, width of excitation region and many others. However, if measuring the linewidth is desired, even greater care (compared to SpBS) has to be taken to ensure accurate measurements are made.

One of the most important attributes of SpBS is that it is easily implemented in a backscattering geometry. This is of great importance when samples are opaque at the laser wavelengths one has available. ISBS in a backscattering geometry is not realizable to measure the interior of bulk samples. However, ISBS has been realized for surfaces in a reflection geometry, and since some biological samples are very thin, such as single cells, the requirement of a transmission configuration is not a prohibiting factor in some cases.

Our inclusion of two different pulse lengths arises from the fact that there are several effects that different pulse lengths have on SBS, and hence ISBS. It has been shown [44] that the SBS threshold increases as the pulse length decreases. In our experiments, the focused peak intensities of the nanosecond and picosecond beams were $I_{nano,Exp} = 6.7 \times 10^7$ W/cm^2 and $I_{pico,Exp} = 1.1 \times 10^{10}$ W/cm^2. Using equations from [44] (Ch. 2) and assuming temporally rectangular pulses we find that the theoretical ratio of the threshold intensities for 6 picosecond and 1 nanosecond pulses should be $\frac{I_{pico,Th}}{I_{nano,Th}} \simeq 160$. In our experiments, the ratio between our two pulse lengths was $\frac{I_{pico,Exp}}{I_{nano,Exp}} \simeq 166$. We observed that our picosecond data had a slightly larger amplitude for equal powers compared to the nanosecond data, which is expected since our ratio was slightly larger than theoretically required. We noticed no other statistical differences between the two pulse lengths in our study.

Because of this threshold dependence on pulse length, there are usually trade-offs when choosing a pulse length for ISBS generation. Ultra-short pulses can induce other nonlinear effects before or at the SBS threshold, which may or may not be desired. Long pulses have a lower threshold, but they also are more prone to cause thermal damage in a sample. We also note that in order for ISBS to be considered impulsive, the pulse length must be shorter than the generated phonon frequency.

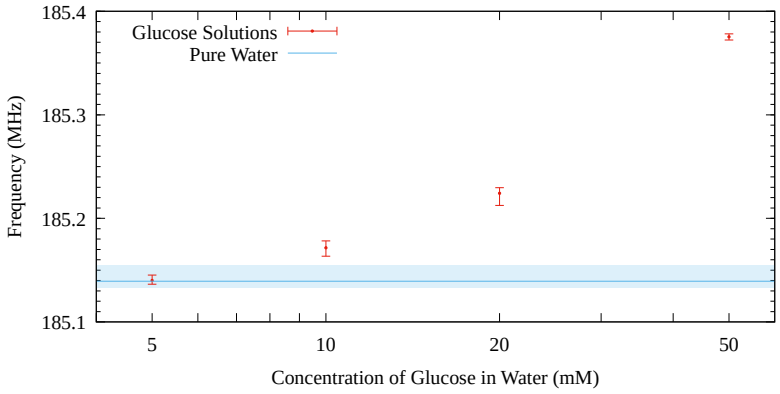

Fig. 5. Measured ISBS frequencies of aqueous glucose solutions at different concentrations. The thin blue line is the pure water reference and the thick translucent blue line is the corresponding pure water error.

Biomedical Optics EXPRESS

As an example of the speed and accuracy of ISBS, we performed an experiment using 532 nm, 1 nanosecond excitation pulses in aqueous glucose solutions at different molar concentrations. Each data point is the average of 5 measurements made, each with 2048 samples (Laser repetition rate is 100kHz) with a pump power of 700 mW. The results are shown in Fig. 5. The presence of glucose in water increases the observed ISBS frequency with increasing concentration. Previous measurements [45, 46] showed the challenges of measuring small Brillouin frequency shifts in solutions of varying chemical content. Glucose (and other small molecules) is present in most biological fluids at mM concentrations, and its concentration is varied dramatically over the course of the day and is often affected by a physiological condition, in particular diabetes. Thus, it becomes crucially important to compare the attained sensitivity of ISBS Brillouin shift measurements with the expected Brillouin shift under typical physiological conditions. The thin blue line in Fig. 5 is the pure water reference frequency measured with our setup (48 μm transmission grating period). The thick translucent blue line marks the error of the pure water measurement. We see that at 5 mM, we were not able to distinguish it from pure water with our current setup. However, a 10 mM concentration can be confidently discerned. Since one measurement takes $\simeq$ 20 ms, this could be used to perform sensitive and fast measurements of transparent samples.

6. Conclusion

In conclusion, we have performed a comparison between CW SpBS and ISBS spectroscopies, in which we utilized 1 ns and 6 ps pump pulses. We measured the Allan variance as a function of time and determined a rough estimate of how many samples were needed in our experiment to accurately determine the SpBS and ISBS frequency for the given accuracy. We demonstrated that ISBS is superior in terms of Brillouin frequency measurements stability and can be used for assessing biologically relevant solutions for physiologically significant chemical variations. As any nonlinear optical spectroscopy, the ISBS signal originates from the focal volume and is not affected, except for its magnitude, by scattering. Several improvements to the current ISBS setup, which will achieve better spatial resolution and even stronger signal, are underway and will be reported elsewhere.

Funding

National Science Foundation (NSF) (DBI-1455671, DBI-1532188, ECCS-1509268, CMMI-#1826078); the Air Force Office of Scientific Research (AFOSR) (FA9550-15-1-0517, FA9550-18-1-0141); the Defense Advanced Research Projects Agency (DARPA) (FA8650-13-D-6368/0006); the Office of Naval Research (ONR) (N00014-16-1-2578); the National Institutes of Health (NIH) (1R01GM127696-01).

Acknowledgments

C. W. B. was supported by the Herman F. Heep and Minnie Belle Heep Texas A&M University Endowed Fund held/administered by the Texas A&M Foundation.

Disclosures

The authors declare that there are no conflicts of interest related to this article.

References

1. E. Jonietz, "Mechanics: The forces of cancer," Nature **491**, S56–S57 (2012).
2. S. Suresh and G. Bao, "Cell and molecular mechanics of biological materials," Nat. Mater. **2**, 715–25 (2003).
3. T. Savin, N. A. Kurpios, A. E. Shyer, P. Florescu, H. Liang, L. Mahadevan, and C. J. Tabin, "On the growth and form of the gut," Nature **476**, 57 (2011).

Biomedical Optics EXPRESS

4. J. Blacher and M. E. Safar, "Large-artery stiffness, hypertension and cardiovascular risk in older patients," Nat. Clin. Pract. Cardiovasc. Med. **2**, 450–455 (2005).
5. A. C. Oates, N. Gorfinkiel, M. Gonzalez-Gaitan, and C.-P. Heisenberg, "Quantitative approaches in developmental biology," Nat. Rev. Genet. **10**, 517–530 (2009).
6. P. G. Gillespie and R. G. Walker, "Molecular basis of mechanosensory transduction," Nature **413**, 194 (2001).
7. W. H. Roos, R. Bruinsma, and G. J. L. Wuite, "Physical virology," Nat. Phys. **6**, 733 (2010).
8. R. Langer and D. A. Tirrell, "Designing materials for biology and medicine," Nature **428**, 487–492 (2004).
9. J. F. Greenleaf, M. Fatemi, and M. Insana, "Selected methods for imaging elastic properties of biological tissues," Annu. Rev. Biomed. Eng. **5**, 57–78 (2003).
10. I. L. Fabelinskii, *Molecular Scattering of Light* (Plenum Press, 1968).
11. J. Randall, J. M. Vaughan, and S. Cusak, "Brillouin Scattering in Systems of Biological Significance [and Discussion]," Philos. T. R. Soc. S-A **293**, 341–348 (1979).
12. Z. Meng, A. J. Traverso, C. W. Ballmann, M. Troyanova-Wood, and V. V. Yakovlev, "Seeing cells in a new light: a renaissance of Brillouin spectroscopy," Adv. Opt. Photonics **8**, 300–327 (2016).
13. K. J. Koski and J. L. Yarger, "Brillouin imaging," Appl. Phys. Lett. **87**, 061903 (2005).
14. G. Scarcelli, W. J. Polacheck, H. T. Nia, K. Patel, A. J. Grodzinsky, R. D. Kamm, and S. H. Yun, "Noncontact three-dimensional mapping of intracellular hydromechanical properties by Brillouin microscopy," Nat. Methods **12**, 1132–1134 (2015).
15. Z. Meng, S. C. Bustamante Lopez, K. E. Meissner, and V. V. Yakovlev, "Subcellular measurements of mechanical and chemical properties using dual Raman-Brillouin microspectroscopy," J. Biophotonics **9**, 201–207 (2015).
16. G. Antonacci, R. M. Pedrigi, A. Kondiboyina, V. V. Mehta, R. de Silva, C. Paterson, R. Krams, and P. Torok, "Quantification of plaque stiffness by Brillouin microscopy in experimental thin cap fibroatheroma," J. R. Soc. Interface **12** (2015).
17. G. Lepert, R. M. Gouveia, C. J. Connon, and C. Paterson, "Assessing corneal biomechanics with Brillouin spectro-microscopy," Faraday Discuss. **187**, 415–428 (2016).
18. G. Antonacci and S. Braakman, "Biomechanics of subcellular structures by non-invasive Brillouin microscopy," Sci. Rep. **6**, 37217 (2016).
19. S. Mattana, M. Mattarelli, L. Urbanelli, K. Sagini, C. Emiliani, M. D. Serra, D. Fioretto, and S. Caponi, "Non-contact mechanical and chemical analysis of single living cells by microspectroscopic techniques," Light. Sci. Appl. **7**, 17139 (2018).
20. K. Elsayad, S. Werner, M. Gallemí, J. Kong, E. R. Sánchez Guajardo, L. Zhang, Y. Jaillais, T. Greb, and Y. Belkhadir, "Mapping the subcellular mechanical properties of live cells in tissues with fluorescence emissionâĂŞBrillouin imaging," Sci. Signal. **9**, rs5 LP – rs5 (2016).
21. Z. A. Steelman, A. C. Weems, A. J. Traverso, J. M. Szafron, D. J. Maitland, and V. V. Yakovlev, "Revealing the glass transition in shape memory polymers using Brillouin spectroscopy," Appl. Phys. Lett. **111**, 241904 (2017).
22. M. Troyanova-Wood, C. Gobbell, Z. Meng, A. A. Gashev, and V. V. Yakovlev, "Optical assessment of changes in mechanical and chemical properties of adipose tissue in diet-induced obese rats," J. Biophotonics **10**, 1694–1702 (2017).
23. Z. Meng, T. Thakur, C. Chitrakar, M. K. Jaiswal, A. K. Gaharwar, and V. V. Yakovlev, "Assessment of Local Heterogeneity in Mechanical Properties of Nanostructured Hydrogel Networks," ACS Nano **11**, 7690–7696 (2017).
24. D. Akilbekova, V. Ogay, T. Yakupov, M. Sarsenova, B. Umbayev, A. Nurakhmetov, K. Tazhin, V. V. Yakovlev, and Z. N. Utegulov, "Brillouin spectroscopy and radiography for assessment of viscoelastic and regenerative properties of mammalian bones," J. Biomed. Opt. **23**, 1–11 (2018).
25. C. W. Ballmann, J. V. Thompson, A. J. Traverso, Z. Meng, M. O. Scully, and V. V. Yakovlev, "Stimulated Brillouin Scattering Microscopic Imaging," Sci. Rep. **5**, 1–7 (2015).
26. I. Remer and A. Bilenca, "Background-free Brillouin spectroscopy in scattering media at 780 nm via stimulated Brillouin scattering," Opt. Lett. **41**, 926–929 (2016).
27. H. Eichler and H. Stahl, "Time and frequency behavior of sound waves thermally induced by modulated laser pulses," J. Appl. Phys. **44**, 3429–3435 (1973).
28. A. A. Maznev, K. A. Nelson, and J. A. Rogers, "Optical heterodyne detection of laser-induced gratings," Opt. Lett. **23**, 1319–1321 (1998).
29. Z. Meng, G. I. Petrov, and V. V. Yakovlev, "Flow cytometry using Brillouin imaging and sensing via time-resolved optical (BISTRO) measurements," Analyst **140**, 7160–7164 (2015).
30. C. W. Ballmann, Z. Meng, A. J. Traverso, M. O. Scully, and V. V. Yakovlev, "Impulsive Brillouin microscopy," Optica **4**, 124–128 (2017).
31. R. Arora, G. I. Petrov, and V. V. Yakovlev, "Analytical capabilities of coherent anti-Stokes Raman scattering microspectroscopy," J. Mod. Opt. **55**, 3237–3254 (2008).
32. Z. Meng and V. V. Yakovlev, "Precise Determination of Brillouin Scattering Spectrum Using a Virtually Imaged Phase Array (VIPA) Spectrometer and Charge-Coupled Device (CCD) Camera," Appl. Spectrosc. **70**, 1356–1363 (2016).
33. Z. Coker, M. Troyanova-Wood, A. J. Traverso, T. Yakupov, Z. N. Utegulov, and V. V. Yakovlev, "Assessing performance of modern Brillouin spectrometers," Opt. Express **26**, 2400–2409 (2018).
34. L. Brillouin, "Diffusion de la lumiere et des rayonnes X par un corps transparent homogene; influence del'agitation

Biomedical Optics EXPRESS

thermique," Ann. Phys. (Paris) **17**, 88–122 (1922).
35. H. Boersch and H. Eichler, "Beugung an einem mit stehenden Lichtwellen gepumpten Rubin," Zeitschrift für Angewandte Physik **22**, 378 (1967).
36. H. J. Eichler, P. Günter, and D. W. Pohl, *Laser-induced dynamic gratings,* Springer series in optical sciences: v. 50 (Springer-Verlag, 1986).
37. J. A. Rogers, M. Fuchs, M. J. Banet, J. B. Hanselman, R. Logan, and K. A. Nelson, "Optical system for rapid materials characterization with the transient grating technique: Application to nondestructive evaluation of thin films used in microelectronics," Appl. Phys. Lett. **71**, 225 (1997).
38. Z. Meng, A. J. Traverso, and V. V. Yakovlev, "Background clean-up in Brillouin microspectroscopy of scattering medium," Opt. Express **22**, 144–148 (2014).
39. A. J. Traverso, J. V. Thompson, Z. A. Steelman, Z. Meng, M. O. Scully, and V. V. Yakovlev, "Dual Raman-Brillouin Microscope for Chemical and Mechanical Characterization and Imaging," Anal. Chem. **87**, 7519–7523 (2015).
40. D. W. Allan, "Statistics of Atomic Frequency Standards," Proc. IEEE **54**, 221–230 (1966).
41. V. V. Yakovlev, "Advanced instrumentation for non-linear Raman microscopy," J. Raman Spectrosc. **34**, 957–964 (2003).
42. J. N. Bixler, B. H. Hokr, M. L. Denton, G. D. Noojin, A. D. Shingledecker, H. T. Beier, R. J. Thomas, B. A. Rockwell, and V. V. Yakovlev, "Assessment of tissue heating under tunable near-infrared radiation," J. Biomed. Opt. **19**, 70501 (2014).
43. J. N. Bixler, B. H. Hokr, C. A. Oian, G. D. Noojin, R. J. Thomas, and V. V. Yakovlev, "Assessment of tissue heating under tunable laser radiation from 1100 nm to 1550 nm," arXiv e-print p. 1509.08022 (2015).
44. B. Y. Zel'dovich, N. F. Pilipetsky, and V. V. Shkunov, *Principles of Phase Conjugation*, vol. 42 (Springer-Verlag Berlin Heidelberg GmbH, 1985).
45. Z. Steelman, Z. Meng, A. J. Traverso, and V. V. Yakovlev, "Brillouin spectroscopy as a new method of screening for increased CSF total protein during bacterial meningitis," J. Biophotonics **8**, 408–414 (2015).
46. J. Garbrecht, H. Hornegger, S. Herbert, T. Kaufmann, J. Gotzmann, K. Elsayad, and D. Slade, "Simultaneous dual-channel imaging to quantify interdependent protein recruitment to laser-induced DNA damage sites," Nucl. (Austin, Tex.) **9**, 474–491 (2018).